JOURNAL OF AIRCRAFT
Vol. 38, No. 2, March–April 2001

Buffet Alleviation on Swept and Unswept Wings at High Incidence

G. A. Flynn,* J. F. Morrison,† and D. G. Mabey‡
Imperial College, London, England SW7 2BY, United Kingdom

Buffeting measurements have been made on semirigid swept and unswept wings with a GA(W)-1 section, at Reynolds numbers Re_c up to 10^6. Results show that a permeable surface, vented to an otherwise airtight plenum, reduces the severity of the buffet excitation. Air passing through the plenum reduces the amplitude of the unsteady separation point. However, the separation is highly three dimensional, producing stall cells and foci of surface-normal vorticity. Qualitative evidence suggests that the buffet excitation parameter increases rapidly when the size of the stall cell approximately doubles and the projected area of separated flow adjacent to the wing increases abruptly. The use of a segmented model ensures that the wing is sufficiently flexible to retain the first bending-moment mode shape. It also allows the position of the permeable surface to be moved to follow the mean separation line approximately. Measurements show significant attenuation of the buffet excitation parameter, by as much as two-thirds, for optimally aligned permeable surfaces. However, in attached flow the permeable surfaces increase buffet excitation, and, when placed in a region of large favorable pressure gradient near the leading edge, separation occurs farther upstream causing an even larger increase in buffet excitation.

Nomenclature

AR	=	aspect ratio, s/c
c	=	wing chord
$F(n)$	=	power spectral density of surface pressure fluctuation
f	=	frequency, Hz
m	=	modal mass
n	=	reduced frequency, $f(c/U_\infty)$
p	=	surface pressure fluctuation
q	=	freestream dynamic pressure
S	=	wing plan area
s	=	span
U_∞	=	freestream velocity
Z	=	mode shape, z/δ
z	=	wing displacement
$\ddot{z}$	=	rms tip acceleration
α	=	angle of incidence
δ	=	wing tip deflection
ζ	=	total damping as a fraction of critical
η	=	fraction of wingspan
Λ	=	sweep angle

Introduction

THE performance of many aircraft components is influenced by flow separation. Important areas are the buffet-onset boundaries for wings at cruise conditions or the onset of buffeting on flaps when deflected for landing. An inevitable concomitant of such separation is buffet excitation; its alleviation by passive means is highly desirable. Raghunathan et al.[1] have shown how the performance of a wide-angled diffuser can be improved by a series of buffet-breather tubes: The pressure fluctuations are reduced and the mean pressure recovery increased. More recently, Heenan and Morrison[2,3] have shown how the separated region downstream of a backward-facing step can be modified by using a permeable surface at reattachment to stabilize separation and, thus, reduce the excitation. Significantly, this passive control reduced the drag as well as the buffet excitation. Both of these experiments suggest that passive control could be applied successfully to reduce the severity of wing and flap buffeting (but not its onset). A companion paper[4] reports preliminary buffet measurements made on a semirigid, unswept integral wing of aspect ratio equal to 3 and $Re_c = 5 \times 10^5$, with fixed transition. It reports the attenuation of the buffet excitation parameter by up to 20% using permeable surfaces beneath the separated flow. The chordwise position of the permeable plates was not optimized. In this paper, the design of a segmented model is outlined that provides the correct first bending-moment mode shape. Results of buffet excitation obtained using this model at Reynolds numbers Re_c up to 10^6 are presented.

Previous buffet research[5–7] has considered buffet loads as a simple linear process in which the buffeting of a semirigid wing is treated as the response of a single resonant mode in a multi-degree-of-freedom system subject to broadband random excitation. Thus, the wing loading is taken to be independent of its motion, and a linear model is adequate. Therefore, the wing deflection must be small, and the induced forces influence the response only though their effect on aerodynamic damping. Jones[7] notes that the limits to these assumptions have not yet been clarified and that nonlinearity plays an essential role in the transfer of energy from the airflow to the wing. It is here that buffet differs from nonlinear flutter, in which nonlinear energy transfer now involves the wing motion in addition to that of the air and which can sometimes be modeled by a limit-cycle oscillation. Stall flutter is most likely to occur when the regular vortex-shedding (Strouhal) frequency excites a natural frequency of the wing. In the case of buffeting, however, turbulent pressure fluctuations cause broadband excitation that is significant across the expected range of structural frequencies, and, therefore, buffet excitation forces can be studied experimentally using a rigid, semirigid, or aeroelastic model.

The use of a rigid model requires the measurement of pressure fluctuations at numerous positions across the wing, and a buffeting coefficient can then be obtained by integrating over the wing surface. With a semirigid or aeroelastic wing, the buffet excitation may be obtained from measurements of the wing response using either root strain gauges or a wing tip accelerometer. This is much more efficient than rigid wing tests. Aeroelastic models tend to be complicated and expensive to build. Thus, semirigid models are the most common for use in buffet research; the model is designed so that the lower-order modes imitate those found in buffeting on aircraft wings or flaps.

For a semirigid cantilevered wing, the buffet excitation parameter can be defined as[5,6,8]

$$\sqrt{nG(n)} = \left(2/\sqrt{\pi}\right)(m\ddot{z}/qS)\zeta^{\frac{1}{2}} \tag{1}$$

Received 20 November 1999; revision received 9 October 2000; accepted for publication 21 October 2000.

*Research Associate, Department of Aeronautics; currently Senior Aircraft Performance Engineer, Aircraft Test and Evaluation Sector, Applied Performance and Requirements Group, Defence Evaluation and Research Agency, Boscombe Down, Salisbury, Wilts, England SP4 0JF, United Kingdom.

†Senior Lecturer, Department of Aeronautics.

‡Visiting Professor, Department of Aeronautics.

Table 1 Levels of buffeting as defined by Mabey[8]

Level	$\sqrt{[nG(n)]}$
Light	0.00075–0.00150
Moderate	0.00150–0.00300
Heavy	>0.00300

where n is the reduced resonant frequency. Equation (1) allows calculation of the (non-dimensional) resultant generalized force where all of the terms on the right-hand side are known. For a wide range of tapered wings, Mabey[8] defines levels of buffeting corresponding to the value of $\sqrt{[nG(n)]}$ as shown in Table 1. In this work, the model was designed so that $\sqrt{[nG(n)]}$ was as large as possible. Overall design constraints determined that values of $\sqrt{[nG(n)]}$ at which significant attenuation was observed lay in the moderate or heavy regimes. Thus, any reductions in $\sqrt{[nG(n)]}$ caused by the permeable surfaces can be measured with an acceptable degree of accuracy.

In this form, the buffet excitation parameter can be compared directly with a dimensionless pressure spectrum in the form proposed by Owen[9]:

$$\frac{\overline{p^2}}{q^2} = \int_0^\infty F(n)\,\mathrm{d}n = \int_0^\infty nF(n)\,\mathrm{d}(\log n) \qquad (2)$$

where n is the general reduced frequency, $\sqrt{[nF(n)]}$ is the (dimensionless) rms intensity of the aerodynamic excitation (a measure of the energy of the excitation at the measurement point), and $\sqrt{[nG(n)]}$ is the integrated response of the wing.

The next section outlines the novel design of a segmented model that provides the correct mode shape closely corresponding to that found on aircraft wings. Subsequently, flow regimes in which there is significant attenuation (as well as amplification) of buffeting are identified, and an attempt is made to relate these to the behavior of the flow adjacent to the wing. This is achieved by measurements of both $\sqrt{[nG(n)]}$ and $\sqrt{[nF(n)]}$ close to the permeable surfaces as well as surface oil-flow visualization. Results for both unswept and swept ($\Lambda = 20$ deg) wings are reported.

Apparatus

Figure 1 shows the experimental rig and the segmented model construction. It comprises a two-dimensional unswept wing with a GA(W)-1 (17% thick) profile[10] and aspect ratio of 2.62. This profile was selected to ensure a benign stall, thus providing a large range of incidence over which the stall could be examined. An integral rigid model of the same section and aspect ratio was also used for chalk/paraffin surface-flow visualization and surface-static pressure measurements. Both wings were optimally tripped using sand grain roughness, that is, the minimum sand grain density and particle size were used to ensure that the initial boundary layer was turbulent. This was checked by using surface-sublimation visualization techniques. The transition was fixed at 5% chord.

These same models were also used for corresponding measurements on a swept wing ($\Lambda = 20$ deg) at similar Reynolds numbers by rotation of the wing in the plane of its chord at zero incidence. Although the wetted surface area remains the same, the aspect ratio is reduced to 2.3. In fact, the sweep angle varies with incidence (because both angle changes are made on the same dividing head), and so these estimates are approximate. Thus, at $\alpha = 16$ deg and $\Lambda = 20$ deg and at $\alpha = 27$ deg and $\Lambda = 18.5$ deg.

To remove the possibility of coupling between the wing and its support, the segmented model was mounted via a dividing head on a seismic mass, the natural frequency of which is significantly lower than that of the first bending mode of the wing (Fig. 1a). The rms tip acceleration was measured by root strain gauges that were calibrated statically in a wind-off test. The calibration constant was then corrected for the difference in deflection shape caused by static and dynamic loads. In earlier tests, $\ddot{z}$ had also been estimated by use of an accelerometer inserted at the tip of the wing; differences

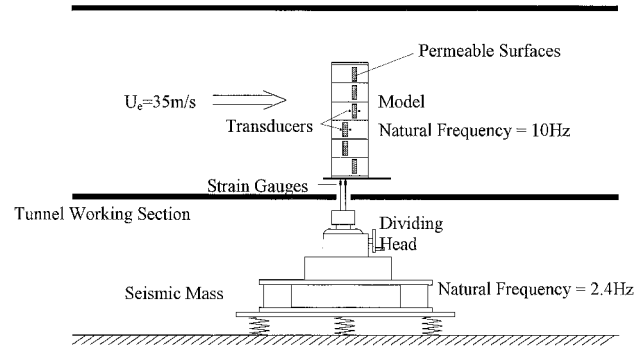

a) Rig assembly

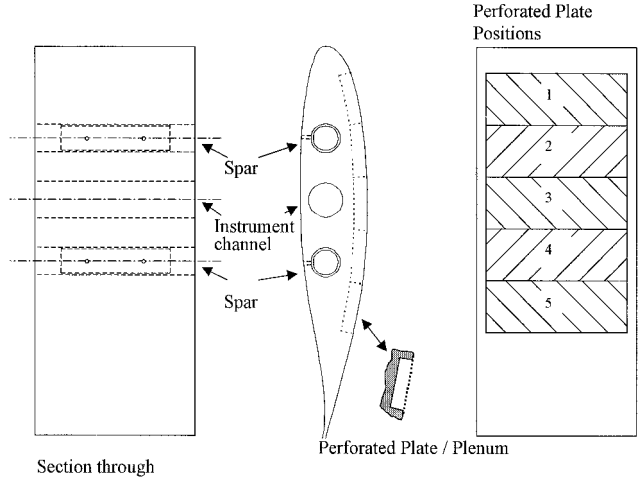

b) Detail of segment construction

Fig. 1 Schematic of segmented model.

in estimates between the two methods were negligible. The modal mass m was calculated assuming a mode shape given by

$$Z = \eta^2 - \tfrac{1}{3}\eta^3 \qquad (3)$$

which satisfies the mechanical boundary conditions. The actual mode shape was checked statically by measuring the change in natural frequency due to the addition of small weights at the wing tip. It is very closely represented by Eq. (3). The damping ratio was estimated during the course of the tests using the random decrement method; thus, the aerodynamic damping is taken to be nonnegligible, although in the present experiments the total damping was small (typically 3% of critical). Zan and Maull[11] discuss the significance of aerodynamic damping: On scaling up to full-size conditions, it is likely that the aerodynamic damping will increase.

For the segmented model, the permeable surfaces (Fig. 1b) are made up of strips of perforated plate with an open-area ratio (OAR) of 22% and circular holes of 1.5-mm diameter. The OAR was selected as being that value above which effects of permeability tend, in a reattaching flow, to saturate.[2] The plenum depth is unlikely to be an optimum; here it is taken to be $0.033c$. Two pressure-fluctuation transducers were also mounted on the surface at different locations. Purpose-built chips that also amplify the output signal were used to drive these. For a fuller description, see Ref. 2. The natural frequency of the model in the first bending mode is 9.8 Hz (with a maximum tip deflection of about 12 mm), whereas that of the seismic mass is 2.4 Hz. No special noise reduction techniques were necessary. However, spikes (of negligible energy) in the wall-pressure spectra are apparent at multiples of the power supply frequency, 50 Hz ($n = 0.43$), and at multiples of the fundamental organ pipe resonance at 86 Hz ($n = 0.74$). The latter also has a prominent subharmonic. Strain gauge and pressure fluctuation data were recorded at 1000 samples/s for 45 s. A 10-min data sample was also recorded, and this showed that results were negligibly different even at very low frequencies.

Finite element analysis was used to design the segmented model. For the spars, a natural frequency of about 10–20 Hz (an order of magnitude greater than that of the seismic mass) was required, with a maximum tip deflection of about 20 mm and a factor of safety of about five for the root-spar loading. Subsequently the wingspan was reduced slightly to increase its natural frequency. Some details of the wing design are important. Its construction comprises a root spar adjoining two wing spars that prevent excessive torsional deflection so that the torsional mode of vibration can be ignored. The measured center of pressure for the wing lies in the range $0.35 < x/c < 0.45$ for the range of incidences over which buffeting is expected to be large, $18 < \alpha < 25$ deg. The positions of the wing spars are $x/c = 0.23$ and 0.55, giving a shear center at about $x/c = 0.4$. Thus, over the range of incidences in question, the torsional mode of vibration is small and at a minimum.

The wing segments (Fig. 1b) are made from a resin mixture with lightweight filler to maximize the natural frequency in bending. This material is also easy to machine. In addition to providing the correct mode shape, this construction also allows a wing to be built so that the position of the permeable surfaces relative to the curved mean separation line can be optimized by inspection of surface-flow visualization photographs obtained using the integral model. However, this segmented design does make it difficult to ensure that the surface is continuous in the spanwise direction. Great care was taken to ensure that sudden changes in surface geometry were kept to an absolute minimum, and the use of cover plates to blank off permeable plates meant that configurations with and without permeable surfaces could be tested without reassembling the model. Thus, there are only minor differences in the datum, that is, no permeable surfaces, estimate of $\sqrt{[nG(n)]}$ from one model build to another. Each configuration is shown with data to which they refer. The permeable surfaces are numbered (1–5), 1 referring to the plate nearest the leading edge. The segments are numbered (1–6), 1 referring to that at the root. Both the integral and segmented models were tested in the same closed-circuit wind tunnel with a working section of 1.37×1.22 m and freestream turbulence intensity of 0.2%.

Results

Table 2 summarizes the principal parameters that characterize each of the configurations used. Individual figures cited in Table 2 include a schematic illustrating the positions of the permeable strips.

Unswept Wing ($\Lambda = 0$ Degree)

The integral model was used to investigate the onset and upstream movement of separation with increasing incidence by means of both surface oil-flow visualization and surface static-pressure measurements at midspan. Figure 2 shows the lift coefficient over the range of incidences and Reynolds numbers of the experiment and illustrates the dependence of rate of stall on Reynolds number. Near zero lift, however, the lift/curve slope for the range of Reynolds numbers used in this work is constant (at about 5.0/rad), indicating that the fixed-position trip is effective. McGhee and Beasley[10] quote the lift/curve slope as 6.9/rad for $Re_c \approx 10^7$ and $AR = 1.57$. Hysteresis was apparent in the pressure distributions obtained on the integral model and is, therefore, also apparent in the lift and drag measurements. Very similar behavior for the unswept model was obtained either for $Re_c = 7.5 \times 10^5$ around $\alpha \approx 20$ deg, or for $\alpha \approx 20$ deg around $Re_c = 7.5 \times 10^5$, with a hysteresis envelope extending approximately for $18 < \alpha < 25$ deg. Qualitatively, this appears to be the result of the attachment line passing around to the pressure surface at large incidences. Because of the large favorable pressure gradient and the effectiveness of the trip on the suction surface, the boundary layer does not separate immediately, this not occurring until $\alpha \approx 25$ deg. When α subsequently decreases, the boundary layer does not reattach until $\alpha \approx 18$ deg. McGhee and Beasley[10] do not observe hysteresis, although their Reynolds numbers are much higher, and this effect is undoubtedly Reynolds number (as well as trip) dependent. Whereas it is expected that the motion of the segmented model will modify this behavior, hysteresis is also observed on the buffet excitation/incidence curve and is discussed hereafter. The data of Fig. 2 and the flow-visualization photographs of Fig. 3 are obtained by fixing the tunnel velocity for the appropriate Reynolds number and increasing the incidence. Thus, the wing is not completely stalled until $\alpha \approx 25$ deg.

Table 2 Principal experimental parameters

Configuration	Figures	Re_c	AR	Λ, deg
M	4–7	7.5×10^5	2.62	0
K	8	7.5×10^5	2.62	0
Q	10–12	8.0×10^5	2.31	20

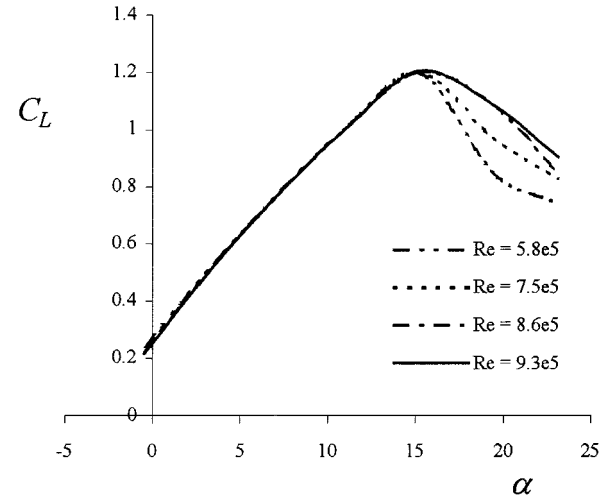

Fig. 2 Lift coefficient vs incidence for a range of Reynolds numbers Re_c.

McGhee and Beasley[10] also show that, at the same Reynolds number, the maximum lift coefficient is about 2.0 at 19 deg, and under these conditions, separation occurs at about 70% of chord. Figure 3 shows surface oil-flow visualizations obtained with the unswept integral model at $Re_c = 7.5 \times 10^5$. A circular end plate is used at the root, but the tip is rounded, as on the segmented model. The top photograph shows that at $\alpha \approx 17$ deg, separation is also at about 70% of chord, although at the lower Reynolds number maximum lift sensibly occurs at lower incidence. For $\alpha > 19$ deg, large variations in the chordwise position of the mean separation line are apparent leading to the formation of mushroom-shaped stall cells. These have received relatively little attention in the published literature, although Gregory et al.,[12] Winkelmann and Barlow,[13] Bippes,[14] and Boiko et al.[15] (who also refer to hysteresis) are exceptions. Weihs and Katz[16] have proposed a model for the formation of stall cells, and, more recently, Yon and Katz[17] have related the stall-cell structure to the generation of pressure fluctuations. In the present work, stall-cell formation is more clearly defined (and more symmetrical about midspan) if an additional tip end plate to the model is used. The cells and the separation foci of surface-normal vorticity appear to be important to the onset and severity of buffeting largely because they determine the area of separated flow adjacent to the wing. The formation of a single large stall cell (from a number of small cells when an additional tip end plate is used) at $\alpha \approx 19$ deg coincides with the large increase in $\sqrt{[nG(n)]}$.

The precise geometry of the stall cell depends on several parameters, including Reynolds number Re_c, AR, the boundary conditions at tip and root, and the nature of the hysteresis in the lift/incidence and lift/Reynolds number relations; more distinct stall cells and foci are apparent for a wing with $AR = 3$ using end plates at the tip as well as at the root. In the present work, there is also evidence (not universally observed) that, at small incidences when the stall cells are small, their span is equal to the chord. Thus, there are three cells when $AR = 3$ and two when $AR = 2$. At larger incidences, the stall cells merge until one single large cell occupies first half and then the whole span. In all of these cases, the preferential wavelength of the disturbance is a multiple of the chord, except where viscous effects dominate, as at the wing/end plate junction. By contrast,

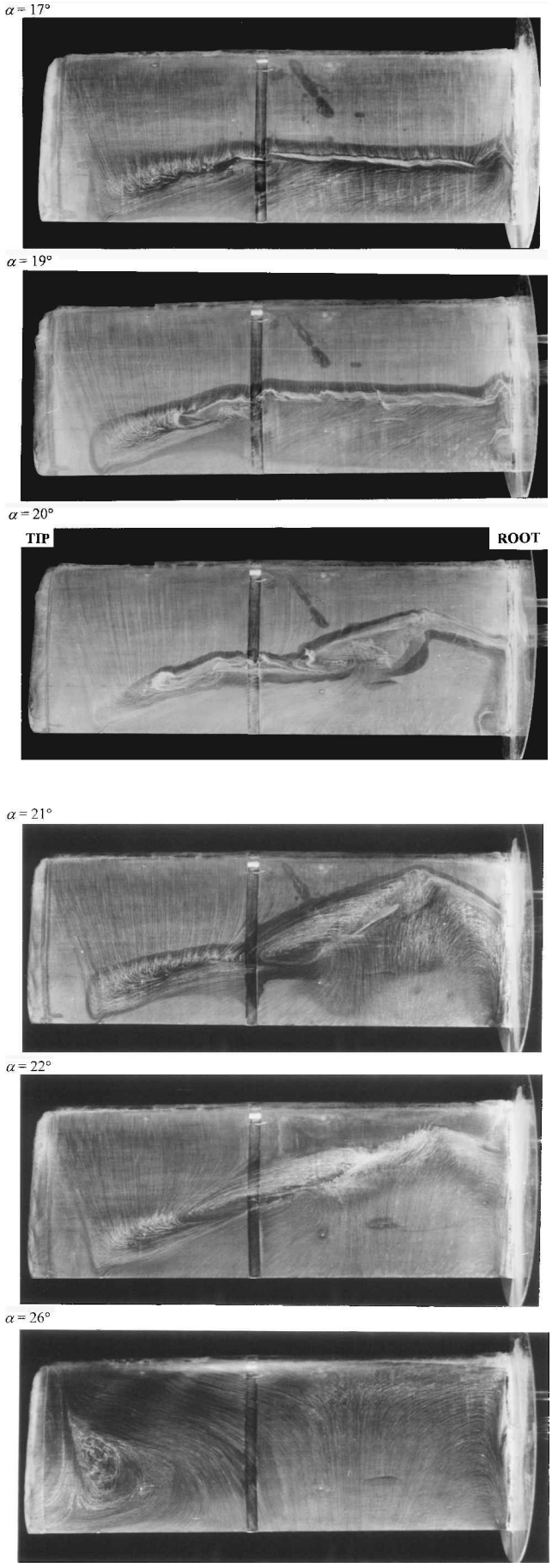

Fig. 3 Oil/chalk surface-flow visualization, $Re_c = 7.5 \times 10^5$ and $\Lambda = 0$, without tip end plate, model mounted vertically.

Winkelmann and Barlow's[13] photographs suggest a wavelength of $3c$. These details, although interesting, are not especially relevant to stall-cell formation on wings with asymmetric boundary conditions undergoing excitation, as in the present work (Fig. 3). Further inspection reveals that, at incidences between about 19 and 21 deg, the position of the separation line (or the leading edge of the stall cell) is unsteady, and its chordwise position varies. This variation can be considerable, and in one test at 20 deg, it changed by as much as $0.13c$. This flicking between two apparently stable states leads to, in one state, a complete stall cell with one edge distorted by the root end plate and, in the other, only half a stall cell with the root end plate located at what would be the center of a full stall cell. Flicking has been observed by previous authors[12] and is likely to contribute to buffet excitation only at very low frequencies ($n < 0.01$).

Figure 4 shows the buffet excitation parameter $\sqrt{[nG(n)]}$ as a function of incidence. These and all subsequent data for $\Lambda = 0$ deg refer to conditions at which the resonant frequency n (in first bending mode) is 0.083 and $Re_c = 7.5 \times 10^5$. For the datum geometry, $\sqrt{[nG(n)]}$ increases slightly in the range $19 < \alpha < 21$ deg as stall cells merge to form one large one. It is in this range that flicking is observed, although not exclusively. At $\alpha \approx 21$ deg, the leading edge of the stall cell coincides with that of the wing, and, subsequently, $\sqrt{[nG(n)]}$ increases rapidly as the stall cell grows across the span. By $\alpha \approx 25$ deg, the wing is fully stalled (Fig. 3), and this condition coincides with the upper bound to the hysteresis envelope. Configuration M refers to the distribution of permeable plates that roughly follow the mean separation line at $\alpha = 20$ deg. Results are shown for both with permeable plates, the distribution of which is shown in the schematic, and without, which is the datum case. They show an attenuation of $\sqrt{[nG(n)]}$ in the range $19 < \alpha < 20$ deg by up to 60%, whereas at smaller incidences, the permeable plates increase it slightly.

Figure 5 shows wall-pressure spectra $\sqrt{[nF(n)]}$ for the same configuration in which measurements were taken at $\alpha = 17$ and 20 deg, that is, at incidences at which $\sqrt{[nG(n)]}$ is increased and reduced, respectively. At $\alpha = 17$ deg, the permeable plates amplify the pressure fluctuations across the whole range of frequencies: Figure 5a is typical, and, in general, the amplification for the higher frequencies is greater downstream of the plate than upstream of it. (Note that the ordinate values change from one transducer position to another.) Figure 5b shows spectra at $\alpha = 20$ deg, one each from a transducer upstream and downstream of segment 3 (numbering from the root). Note that at this incidence, there is a large increase in energy at very low frequencies, $n \approx 0.01$. There is clear attenuation by the permeable plates up to $n \approx 0.3$ both upstream and downstream of the permeable plate, but at higher frequencies, there is significant amplification downstream of the plate. Figure 5b also shows equivalent spectra for segment 4. Here, the upstream spectra are qualitatively the same as those on segment 3, but, downstream of the permeable plate, $\sqrt{[nF(n)]}$ is amplified over the whole frequency range despite the reduction in $\sqrt{[nG(n)]}$. Overall, it is clear that, even in cases in which $\sqrt{[nG(n)]}$ is increased, there can be an attenuation of $\sqrt{[nF(n)]}$ locally and that this is more likely to occur at low frequencies than at high ones. Similarly, for configurations in which $\sqrt{[nG(n)]}$ is reduced, there are regions on the wing surface in which $\sqrt{[nF(n)]}$ has been increased. In fact, the permeable plates tend to amplify $\sqrt{[nF(n)]}$ at higher frequencies, and this effect is larger downstream.

Figure 6 shows measurements of $\sqrt{[nG(n)]}$ obtained during an additional test using a different build (but the same configuration) from that used to obtain the data of Figs. 4 and 5. Comparison of these data with those of Fig. 4 illustrates the difficulty in obtaining repeatability of the data, largely due to unsteadiness of the flowfield at very low frequencies. Even so, the incidence range and degree of attenuation is very similar to that of Fig. 4. It also shows the effect of hysteresis on $\sqrt{[nG(n)]}$ (the incidence is changed without starting or stopping the tunnel). The lower pair of curves show $\sqrt{[nG(n)]}$ as α increases (and are very similar to those in Fig. 4), whereas the upper pair show $\sqrt{[nG(n)]}$ as α decreases. It is clear that the properties of the flow at, for example, $\alpha = 20$ deg, are strongly dependent on whether the incidence in increasing or decreasing. Moreover,

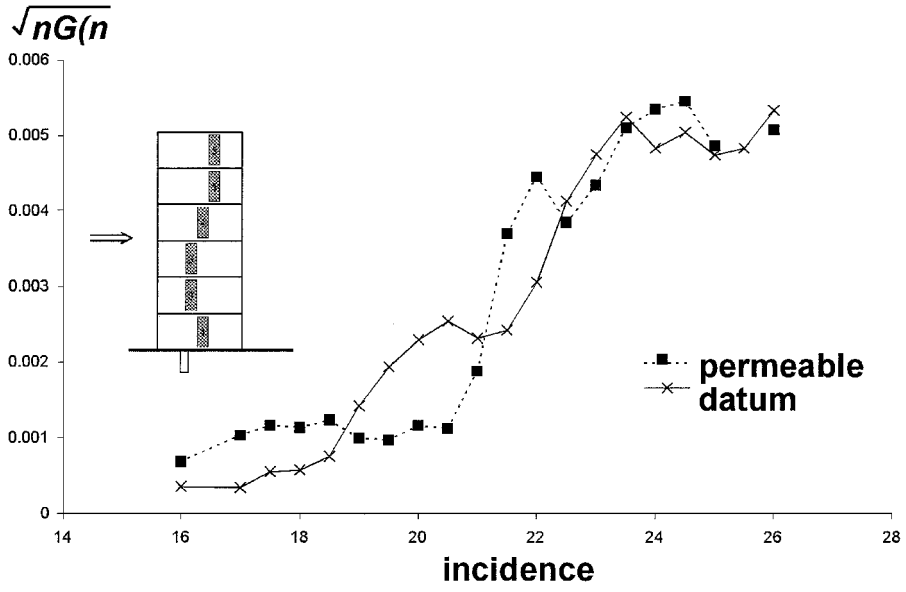

Fig. 4 Configuration M $\sqrt{[nG(n)]}$: ■, permeable, and ×, datum; $n = 0.083$ and $Re_c = 7.5 \times 10^5$.

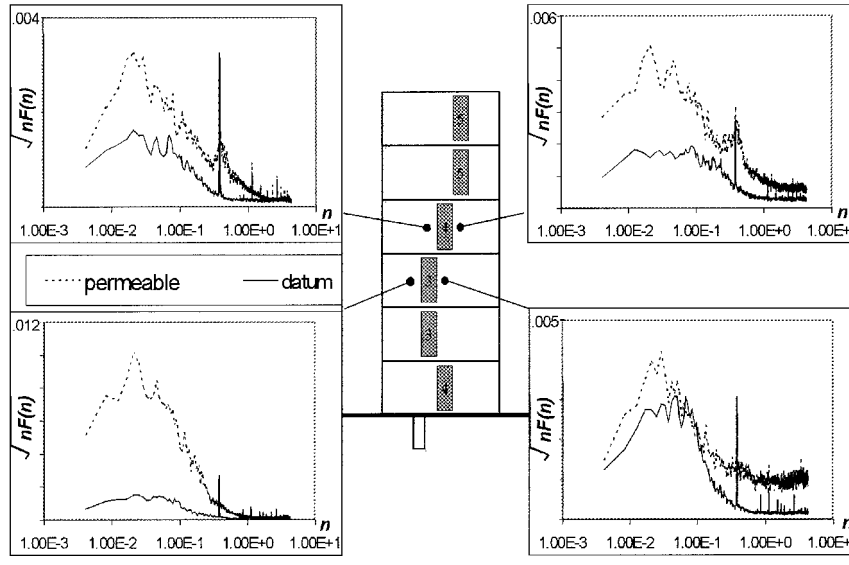

a) $\alpha = 17$ deg

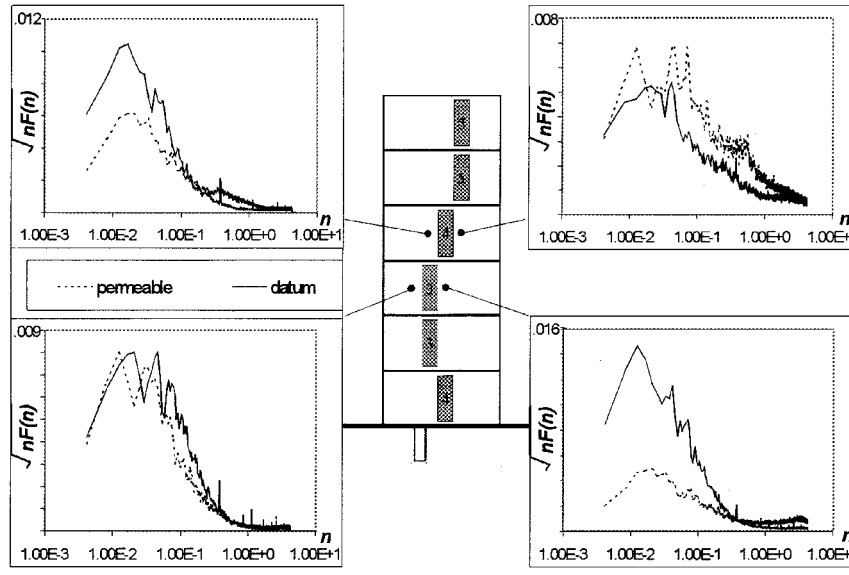

b) $\alpha = 20$ deg

Fig. 5 Surface pressure spectra, $\sqrt{[nF(n)]}$, for configuration M: - - - -, permeable, and ——, datum.

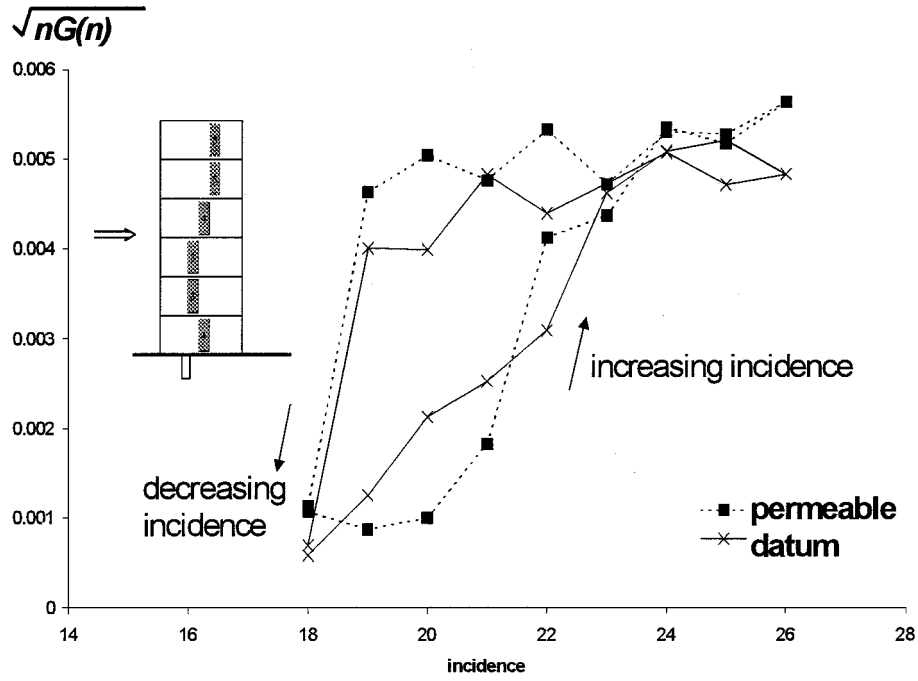

Fig. 6 Configuration M $\sqrt{[nG(n)]}$, demonstration of hysteresis with changing incidence: - - - -, permeable, and ——, datum.

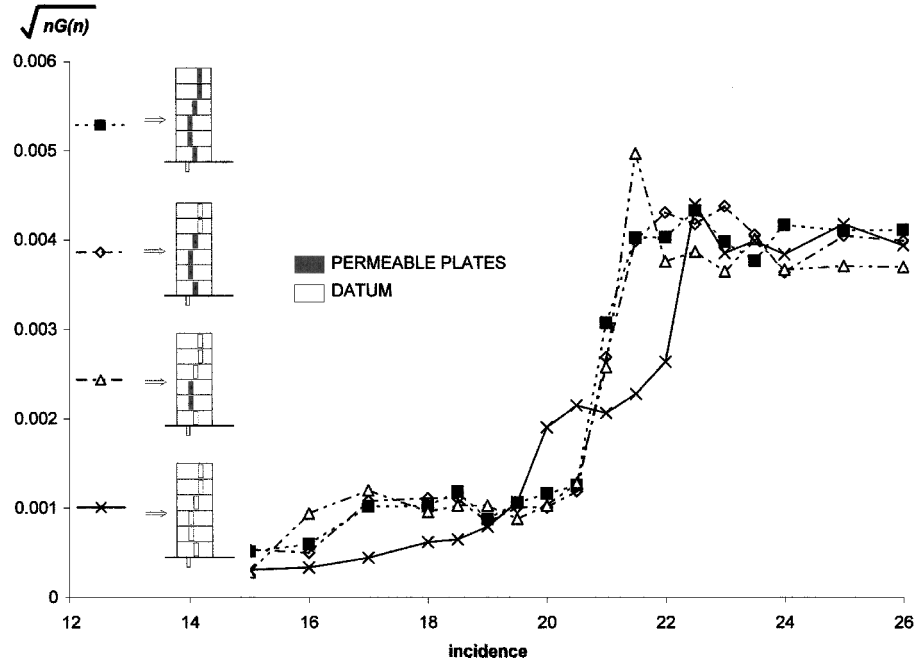

Fig. 7 Configuration M $\sqrt{[nG(n)]}$, effect of successive modifications to distribution of permeable plates: - - - -, permeable, and ——, datum.

only when α is increasing do the permeable plates provide attenuation. Hysteresis effects are also observed with changes in Reynolds number. Results in this work refer to the properties of the lower hysteresis curve in Fig. 6, which, being the more stable flow, is that obtained when the incidence is increased at fixed Reynolds number.

Figure 7 illustrates the effect of modifications to the arrangement of permeable plates introduced by successively masking some of them, as shown. For $\alpha \leq 15$ deg, the initial increase in $\sqrt{[nG(n)]}$ relative to the datum case occurs for two of the modifications and at $\alpha \geq 16$ deg for the other one as well. Thus, the plates nearer the trailing edge become more effective at lower incidences than those near the leading edge. It is clear that the permeable plates on segments 2 and 3 are mainly responsible for the changes in buffet excitation, despite that, due to the mode shape, separated flow over the wing tip contributes proportionately more to the rms tip acceleration and, therefore, to $\sqrt{[nG(n)]}$ also. The observed changes in $\sqrt{[nG(n)]}$ are simply because of the larger wing area at the root exposed to separated flow (Fig. 3).

Figure 8 relates the nature of the flow over the wing to changes in $\sqrt{[nG(n)]}$. Here configuration K is used, which has minor differences compared to configuration M (Fig. 4): Permeable plates in segments 1 and 4 are moved aft to location 5. Flow visualization tests were carried out using minitufts[18] for a range of incidences. Then all of the permeable plates were masked with tape to create the datum case, and the flow visualization was repeated. The suction surface is divided into the following regions: 1) separated, where the tufts clearly indicate a surface flow direction that is opposite to that of the freestream; 2) intermittent, where the tufts' direction

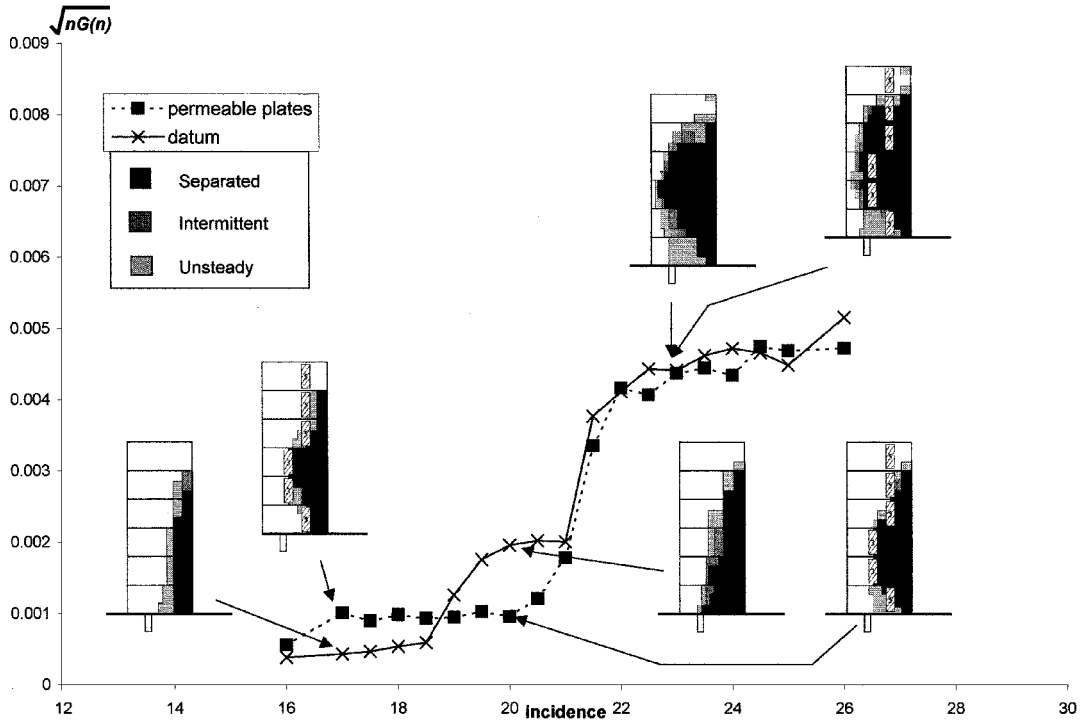

Fig. 8 Configuration K $\sqrt{[nG(n)]}$ with surface flow visualization.

alternates between upstream and downstream directions; and 3) unsteady, where the tufts indicate a direction that is predominantly the same as that of the freestream but is nevertheless highly unsteady.

The motion of the tufts is dominated by their behavior at very low frequencies (1–2 Hz, $n \approx 0.01$), which manifests itself as an unsteadiness in the separation line and which, in the range $19 < \alpha < 21$ deg, includes flicking between different stall-cell patterns. This low-frequency behavior is, therefore, the key discriminator of the three regions. Figure 8 links these observations with the measured buffet excitation parameters. At $\alpha = 17$ deg, it appears that the permeable plates pull the mean separation line upstream to the position of the permeable plate, causing an increase in the area of separated flow and, therefore, in $\sqrt{[nG(n)]}$ also. Otherwise, as α increases, the effect of the permeable plates is to inhibit the growth of the separated region, particularly near the root. Over all incidences, the area of wing surface on which the flow is either intermittent or unsteady is reduced by the permeable plates, producing a steadier separation pattern. It is also evident that the separated region in the datum case is closer to the root. At $\alpha = 21.5$ deg, the separated region for the datum case starts to move outward toward the tip, and differences in the two flows become small, as indeed do the differences in buffet excitation.

For configurations in which the permeable plate in segment 2 or 3 is close to the leading edge, there are increases in $\sqrt{[nG(n)]}$ over the whole range of incidences examined. In particular, $\sqrt{[nG(n)]}$ increases rapidly as the mean separation line reaches the leading edge, where the effect of one (or more) permeable plates is to remove the large favorable pressure gradient present in the datum case. Therefore, the plan area of the wing immediately adjacent to separated flow increases suddenly and, thus, $\sqrt{[nG(n)]}$ also.[4,19] This results in increased levels of buffet excitation for all incidences, but especially over the range of incidence for which attenuation is otherwise expected.

Swept wing (Λ = 20 Degree)

Figure 9 shows results of oil-flow visualization tests performed on the swept-wing model, but for a higher aspect ratio and slightly higher Reynolds numbers. Even so, a qualitative comparison with the photographs of Fig. 3 is in order.

The characteristics of the separation are very different from the unswept case. It is evident that no stall cells are formed, and a

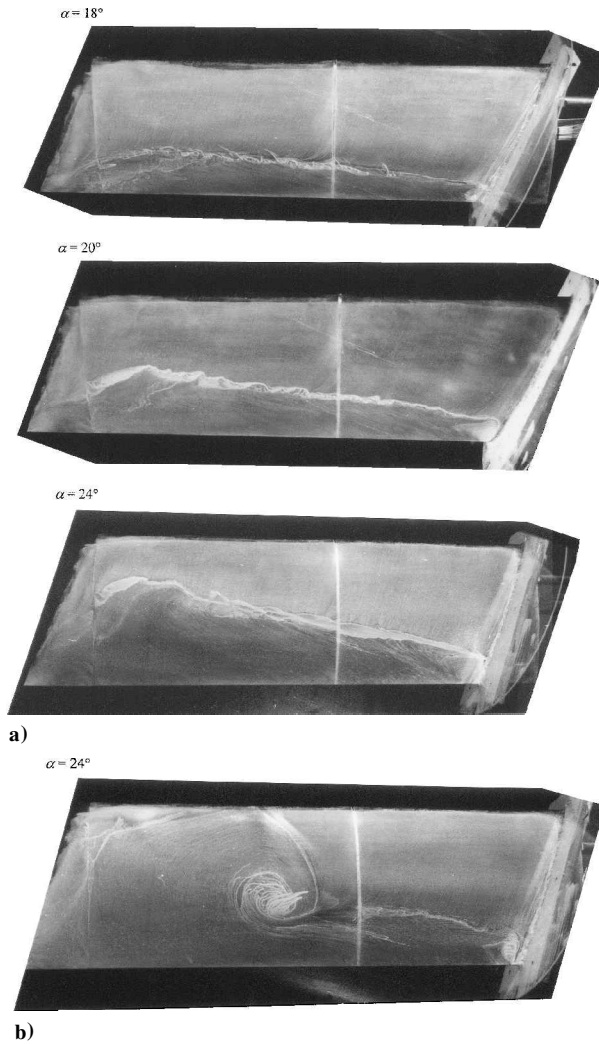

Fig. 9 Oil/chalk surface-flow visualization: a) $Re_c = 9.5 \times 10^5$; AR = 3; Λ = 20 deg; α = 18, 20, and 24 deg and b) $Re_c = 8.0 \times 10^5$, AR = 3, Λ = 20 deg, and α = 24 deg, without tip end plate, model mounted vertically.

focus of separation does not become apparent until $\alpha = 26$ deg at $Re_c = 9.5 \times 10^5$ or $\alpha = 24$ deg at $Re_c = 8 \times 10^5$. Instead, a separation line forms that is almost perpendicular to the freestream direction. Thus, separation occurs earlier near the tip. It is only when the separation line at the tip reaches the wing leading edge, and the area of fully separated flow starts to spread toward the root, that a focus of separation begins to form. Because of the fundamentally different nature of the stall on the swept wing, it is anticipated that permeable plates placed near the wing tip are more likely to accomplish any attenuation of buffet excitation than in the unswept case.

Based on these observations, configuration Q was used to estimate changes in $\sqrt{[nG(n)]}$ over a range of incidences. Figure 10 shows that there is little change in $\sqrt{[nG(n)]}$ at small incidences: There is no increase as in the unswept configurations. However, between $\alpha = 21.5$ and 24 deg there is considerable attenuation (of about 40%), whereas at higher incidences there is an increase in the buffet excitation. Also shown are results obtained when the permeable plate on segment 6 (at the tip) is masked. Then there appears to be little initial effect on $\sqrt{[nG(n)]}$ at lower incidences, yet it is clear that the tip permeable plate is responsible for nearly all of the attenuation between $\alpha = 21.5$ and 24 deg.

The wall-pressure spectra corresponding to the measurements of $\sqrt{[nG(n)]}$ are shown in Fig. 11. At $\alpha = 23$ deg, where there is considerable attenuation, there is also a very large reduction in the level of pressure fluctuations, at all frequencies, upstream of the permeable plate on the fourth segment. On the fifth segment, however, the high-frequency pressure fluctuations are amplified both upstream and downstream of the permeable plate. When the sixth-segment plate is masked, the buffet alleviation is reduced: The low-frequency fluctuations are reduced at all transducer locations whereas the higher frequencies are relatively unchanged. This effect appears to be the result of the attenuation, by the tip permeable plate, of the separating or separated[2,3] large eddies that have pressure-convection velocities toward the root. At $\alpha = 26$ deg (figure not shown) when $\sqrt{[nG(n)]}$ is increased by the permeable plates, there is a large increase in $\sqrt{[nF(n)]}$ across most of the frequency range downstream of the fifth-segment plate, and no attenuation at the other locations. The effect of masking the sixth-segment plate is only to remove the amplification of $\sqrt{[nF(n)]}$ downstream of the fifth-segment plate.

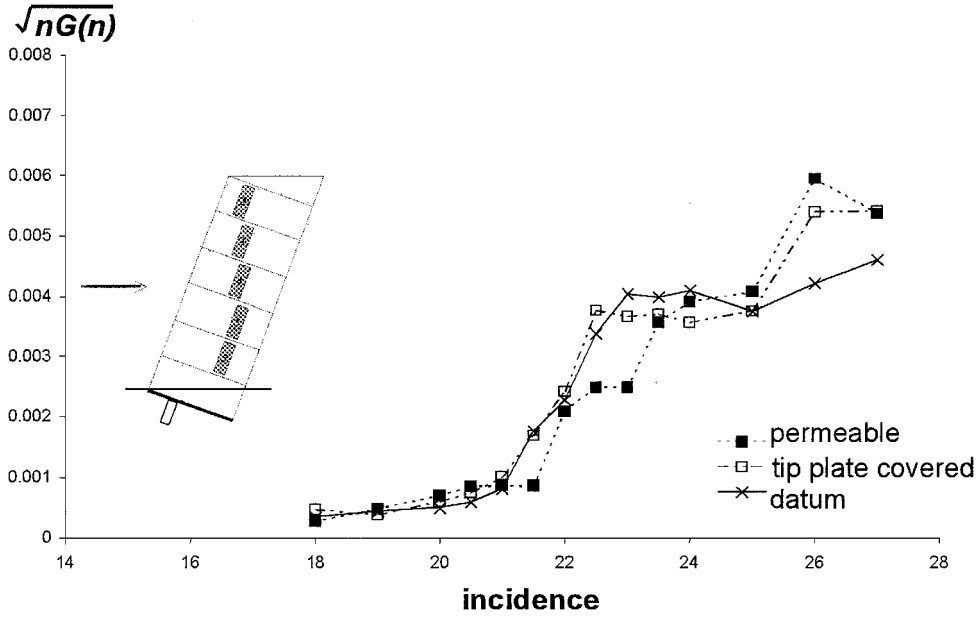

Fig. 10 Configuration Q (swept wing) $\sqrt{[nG(n)]}$: $n = 0.072$, $Re_c = 8.0 \times 10^5$, AR = 2.31, and $\Lambda = 20$ deg with - - - -, permeable; - - — - -, tip plate covered; and ——, datum.

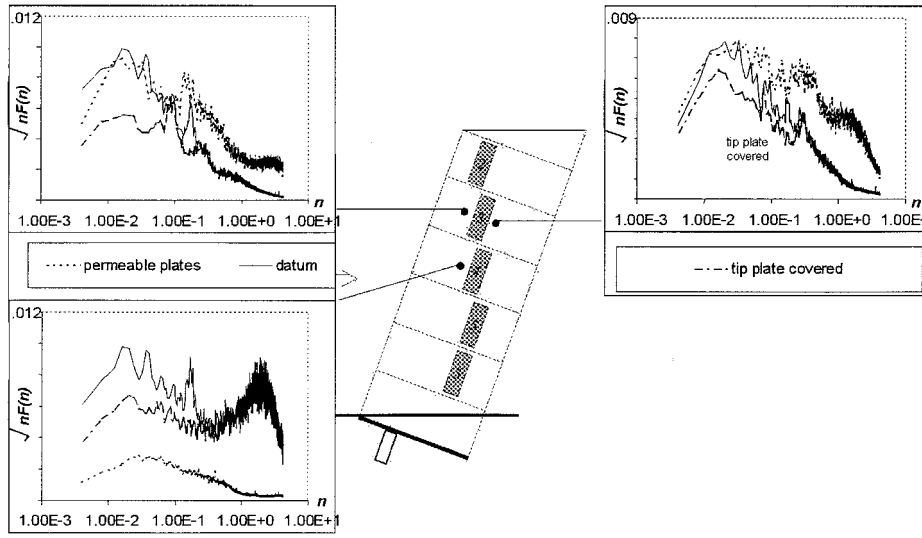

Fig. 11 Surface pressure spectra for configuration Q (swept wing), $\alpha = 23$ deg: - - - -, datum; - — -, tip plate covered; and ——, permeable.

Statement of Measurement Uncertainties

Measurements of $\sqrt{[nG(n)]}$ for some configurations were repeated to estimate the uncertainty of the buffet excitation, which is typically 20% (95% confidence). Repetitive measurements were quite difficult due to the large low-frequency oscillations of the wing both in and out of the chord line plane and their sensitivity to small surface changes from one build to another. Modifications to the segmented model helped by increasing its natural frequency. However, the uncertainty of measurements of $\sqrt{[nG(n)]}$ for the same build were typically 10% (95% confidence). This is obviously also the case for the surface pressure fluctuation data, which were found to be repeatable to within 5% (95% confidence) for the same build.

Discussion

The use of surface-sublimation flow visualization indicates that the sand grain trip (fixed at 5% chord) is fully effective at all, except possibly the largest, incidences. In these cases, there is evidence that transition proceeds via a separation bubble before the trip is reached. In addition, the motion of the wing would suggest that transition proceeds quickly and that it occurs before full separation.

Besides those spikes already discussed and attributed to the acoustic properties of the tunnel, the wall-pressure spectra in Fig. 5 have peaks at $n \approx 0.01$, whereas the buffet frequency corresponds to $n = 0.084$, and the natural frequency of the seismic mass corresponds to $n = 0.02$. There is no identifiable peak for the buffet frequency, which implies that the excitation is indeed broadband, as has been assumed in the analysis leading to Eq. (1). Thus, the motion of the wing does not dominate the pressure-fluctuation field, as would be the case in a limit-cycle oscillation. However, it is likely that the motion of the seismic mass contributes to the low-frequency behavior of these spectra. Unlike the surface-pressure spectra of Yon and Katz,[17] no bluff-body shedding frequency is observed. Here, for $\alpha = 20$ deg, this would occur at $n \approx 0.6$ assuming a Strouhal number of 0.2 and using a length equal to the projected chord of the wing[20] (see Fig. 5b). It is likely that the flow is too disturbed by the wing motion for a discrete vortex-shedding frequency to be distinguishable, although surface-pressure measurements are not necessarily the best indicator of such a process.

Given that $\sqrt{[nF(n)]}$ (as well as the area under the spectra of Figs. 5 and 11) is a spectral measure of the energy of the excitation at a point on the wing, it is clear that, although the excitation is broadband in nature, it predominates at very low frequencies. Gregory et al.,[12] Yon and Katz,[17] and Zaman et al.[21] have all examined the frequencies prevalent in the flow over an aerofoil in deep stall (but before full stall) and suggest that there is a dominant low-frequency oscillation, resulting in a flapping of the separated shear layer. This can originate from flicking also. Zaman et al. suggest that the illusive nature of the phenomenon is due to its dependence on the nature of the boundary layer, which should be in a transitional state, and that the phenomenon is not present when the separating layer is either turbulent or even laminar. In the present work, this would require the trip at 5% chord to be not wholly effective, and this seems unlikely. The visual evidence appears compelling: A low-frequency oscillation including periodic switching between different stages of stall (identifiable in terms of the size and number of stall cells) can occur with turbulent separation. During flow visualization studies on a fixed support (i.e., one that has a natural frequency much higher than that of the seismic mass), very low periodic oscillations of the stall pattern were still observed. In the present work, this occurs for $n \approx 0.01$, which unfortunately coincides with the fundamental frequency of the seismic mass. Thus, we are unable to distinguish unambiguously the cause of this motion and isolate it from that of the seismic mass.

However, the spectra of Fig. 5 show that the low-frequency energy associated with the unsteadiness is largest for $18 \leq \alpha \leq 23$ deg and that this range coincides with a rapid rise in $\sqrt{[nG(n)]}$ for the datum cases. Furthermore, for $\alpha > 23$ deg, the airfoil is fully stalled, $\sqrt{[nG(n)]}$ reaches a plateau, and the forces on the seismic mass are at a maximum. For comparison with Fig. 5, Fig. 12 shows pressure spectra at $\alpha = 24$ deg, when the low-frequency peak in $\sqrt{[nF(n)]}$ at most transducer locations actually decreases, presumably because the separation point is relatively steady and close to the leading edge. Yet, $\sqrt{[nG(n)]}$ does not decrease due to a pronounced increase in $\sqrt{[nF(n)]}$ at high frequencies. This low-frequency motion has also been documented by Yon and Katz.[17] Consistent with this view, Zan and Maull[11] suggest that foci are responsible for excitation at frequencies that are typically an order of magnitude smaller than those associated with buffeting, that is, at frequencies associated with flapping. However, the present results suggest that the major part of the excitation energy exists at these low frequencies.

Because the geometry of apparently stable arrays of stall cells is important to buffet excitation, it is perhaps useful to comment on some of their details, even for the slightly less relevant case in which a tip end plate is used so that the cells are more clearly defined. Of the previous workers who have studied the phenomenon, only Boiko et al.[15] explicitly refer to the reduction in number of cells as the wing proceeds to complete stall, which, for rectangular planforms with end plates, comprises one large cell that is symmetrical about midspan. In the present work and presumably that of Boiko et al.[15] also, this effect has been observable because the stall

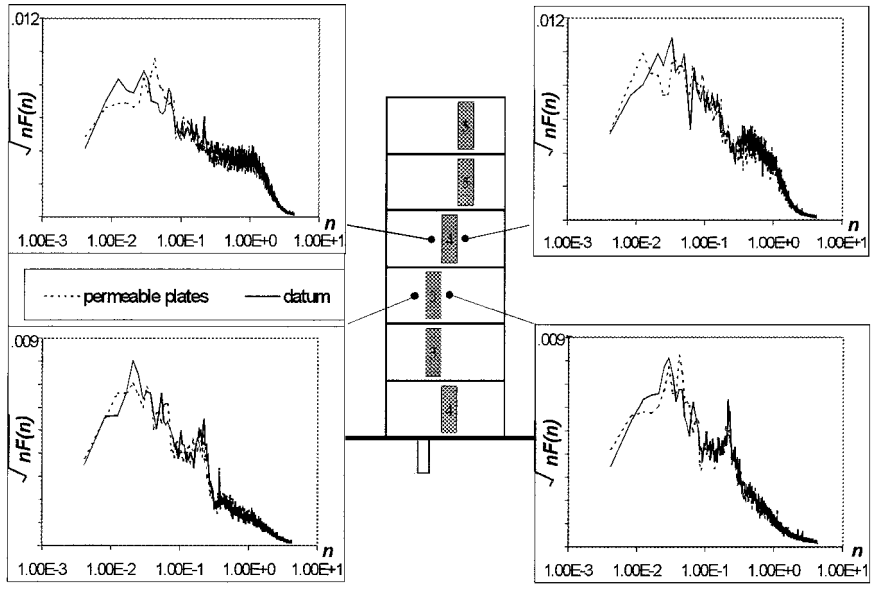

Fig. 12 Surface pressure spectra, $\sqrt{[nF(n)]}$, for configuration M, α = 24 deg: - - - -, permeable, and ——, datum.

occurs slowly. Moreover, in the present work, flow visualization shows that the effect of reducing AR (but with otherwise identical conditions) leaves the sizes of the stall cells at any incidence unchanged. However, this requires the use of adequate end plates that can act as image generators rather than a source of significant viscous effects. Vullierme[22] has recently performed simulations at low Reynolds numbers ($Re_c \approx 10^3$), also with the GA(W)-1 aerofoil, using boundary conditions that are spanwise periodic on a wing for which $AR = 4$. These also show the formation of stall cells with foci of surface-normal vorticity. Using the vortex-eduction scheme of Jeong and Hussain,[23] he illustrates the development of the primary spanwise vortices connected by the secondary braids of streamwise vorticity. With the use of linear calculations, Lin and Corcos[24] (see also Neu[25]) show that when these braids are subject to mutual and self-induction in shear, they collapse into mushroom-shaped vortices. The appearance of stall cells on the wing surface in experiments would suggest that this is also a realistic explanation at high Reynolds numbers, the only prerequisite for such a process being that the strength of the vortex sheet is greater than the square root of the product of the viscosity and strain rate. Simulation data are required to analyze such flows in terms of both their topology (saddle points, foci, and nodes) and their stability.[26,27] Such work would help in the understanding of stall-cell formation and, therefore, offer reasons for the large and sudden increase in $\sqrt{[nG(n)]}$ with incidence.

The static, integral wing exhibits aerodynamic hysteresis in terms of changes in lift coefficient (and pressure distributions) with both incidence and Reynolds number. Figure 6 shows that hysteresis effects appear in buffet excitation also as measured with the segmented model. However, in the latter case, it is likely that structural hysteresis also occurs and that this exacerbates the aerodynamic hysteresis apparent in Fig. 6. As the incidence increases, the increase in static twist is likely to lead to hysteresis behavior in the segmented model. Hysteresis in stall has also been observed by Meyer et al.,[28] who use flexible, permeable flaps for control. It appears that these devices also modify hysteresis effects. Future work should include a detailed study of unsteady separation (and its modification by permeable surfaces) on a rigid wing with minimal extraneous effects so that the stall-cell pattern is well defined. This should involve a study of its effect on both surface-pressure fluctuations and velocity fluctuations in the wake.

Conclusions

A simple technique for the passive attenuation of the buffet excitation parameter has been demonstrated using a semirigid model with a mode shape that approximates that of the first mode in bending on a full-size wing. Earlier work showed that the mean root-bending moment is also reduced. Permeable plates, vented to an airtight plenum, are able to attenuate the low-frequency oscillations of the separating shear layer, so stabilizing the separation point and reducing its amplitude about the mean. A detrimental effect of these devices is that the favorable pressure gradient near the leading edge is removed when plates are sufficiently near the leading edge, thus causing an earlier separation and a much increased buffet excitation parameter. More generally, a plenum tends to increase the static pressure, thereby reducing the lift. In attached flow, a permeable plate increases turbulent mixing and, therefore, drag also. However, it is conceivable that, with an optimized configuration, drag could be reduced along with buffet excitation, as has been achieved for reattaching flow.[2,3]

For $18 \leq \alpha \leq 23$ deg, the attenuation of the surface pressure fluctuations occurs mostly for $n < 0.5$, although immediately downstream of a permeable plate, the high-frequency components of the pressure field are amplified. Low-frequency attenuation of the pressure field is the primary mechanism for the attenuation of $\sqrt{[nG(n)]}$, although the precise way in which this related to the velocity field is not yet clear. Evidence here suggests that permeable plates, correctly positioned, inhibit the low-frequency unsteadiness about the mean separation line and the flapping of the separated shear layer.

The success of these devices suggests that they may find further application in noise-related problems. There are strong hysteresis effects apparent in the buffet excitation parameter. Further work is required to clarify the nature of the lowest-frequency oscillations that are related to flicking between stalled and part-stalled states. Further experiments with both forward and backward swept wings, on which the mechanisms are different from those occurring on unswept wings, would be very useful.

Acknowledgments

This work is supported under Contract ASF/2601U by the Defence Evaluation and Research Agency, Bedford. We are indebted to its Monitor, John L. Fulker. We are grateful to Alexander J. Smits, who was host to J. F. Morrison during his stay at the Department of Mechanical and Aerospace Engineering, Princeton University, when the major part of this paper was written.

References

[1]Raghunathan, S., McIlwain, S. T., and Mabey, D. G., "Wide Angle Diffusers with Passive Boundary-Layer Control," *Aeronautical Journal*, Vol. 95, No. 1, 1991, pp. 28–34.

[2]Heenan, A. F., and Morrison, J. F., "Passive Control of Pressure Fluctuations Generated by Separated Flow," *AIAA Journal*, Vol. 36, No. 5, 1998, pp. 1014–1022.

[3]Heenan, A. F., and Morrison, J. F., "Passive Control of Backstep Flow," *Experimental Thermal and Fluid Science*, Vol. 16, No. 1, 1998, pp. 122–132.

[4]Flynn, G. A., and Morrison, J. F., "Passive Control of Buffet Excitation," *IUTAM Symposium on Mechanics of Passive and Active Flow Control*, edited by G. E. A. Meier and P. R. Viswanath, Kluwer Academic, Norwell, MA, 1999, pp. 63–68.

[5]Huston, W. B., "A Study of the Correlation Between Flight and Wind-Tunnel Buffet Loads," Rept. 111, AGARD, 1957.

[6]Davis, D. D., Jr., and Wornom, D. E., "Buffet Tests of an Attack-Airplane Model with Emphasis on Analysis of Data from Wind-Tunnel Tests," NACA Research Memorandum L57H13, 1958.

[7]Jones, J. G., "A Survey of Dynamic Analysis of Buffeting and Related Phenomena," Royal Aircraft Establishment, TR 72197, 1973.

[8]Mabey, D. G., "Some Aspects of Aircraft Dynamic Loads Due to Flow Separation," *Progress in Aerospace Science*, Vol. 26, 1989, pp. 115–151.

[9]Owen, T. B., "Techniques of Pressure-Fluctuation Measurements Employed in the RAE Low-Speed Wind-Tunnels," Rept. 172, AGARD, 1958.

[10]McGhee, R. J., and Beasley, W. D., "Low-Speed Characteristics of a 17%-Thick Airfoil Section Designed for General Aviation Applications," NASA Technical Note D 7428, 1973.

[11]Zan, S. J., and Maull, D. J., "Buffet Excitation of Wings at Low Speeds," *Journal of Aircraft*, Vol. 29, No. 6, 1992, pp. 1137–1143.

[12]Gregory, N., Quincey, V. G., O'Reilly, C. L., and Hall, D. J., "Progress Report on Observations of Three-Dimensional Flow Patterns Obtained During Stall Development on Aerofoils, and on the Problem of Measuring Two-Dimensional Characteristics," Aeronautical Research Council 1146, 1971.

[13]Winkelmann, A. E., and Barlow, J. B., "Flowfield Model for a Rectangular Planform Wing Beyond Stall," *AIAA Journal*, Vol. 18, No. 8, 1980, pp. 1006–1008.

[14]Bippes, H., "Experimental Investigation of Topological Structures in Three-Dimensional Separated Flow," *Boundary-Layer Separation*, edited by F. T. Smith and S. N. Brown, Springer-Verlag, Berlin, 1987, pp. 379–381.

[15]Boiko, A. V., Dovgal, A. V., Zanin, B. Y., and Kozlov, V. V., "Three-Dimensional Structure of Separated Flows on Wings (Review)," *Thermophysics and Aeromechanics*, Vol. 3, No. 1, 1996, pp. 1–13.

[16]Weihs, D., and Katz, J., "Cellular Patterns in Poststall Flow over Unswept Wings," *AIAA Journal*, Vol. 21, No. 12, 1983, pp. 1757–1759.

[17]Yon, S. A., and Katz, J., "Study of the Unsteady Flow Features on a Stalled Wing," *AIAA Journal*, Vol. 36, No. 3, 1998, pp. 305–312.

[18]Mabey, D. G., Welsh, B. L., and Pyne, C. R., "A Note on the Interpretation of Mini-Tuft Photographs," *Aeronautical Journal*, Vol. 32, No. 5, 1995, pp. 178–182.

[19]Flynn, G. A., Morrison, J. F., and Mabey, D. G., "Buffet Alleviation on an Unswept Wing at High Incidence," AIAA Paper 99-0791, Jan. 1999.

[20]Mabey, D. G., "Similitude Relations for Buffet and Wing Rock on Delta Wings," *Progress in Aerospace Sciences*, Vol. 33, 1997, pp. 481–511.

[21]Zaman, K. B. M. Q., McKinzie, D. J., and Rumsey, C. L., "A Natural Low-Frequency Oscillation of the Flow over an Airfoil Near Stalling Conditions," *Journal of Fluid Mechanics*, Vol. 202, 1989, pp. 403–442.

[22]Vullierme, A. N., "Computational Modelling of Buffeting," M.S. Project Rept., Dept. of Aeronautics, Imperial College, London, 1999.

[23]Jeong, J., and Hussain, F., "On the Identification of a Vortex," *Journal of Fluid Mechanics*, Vol. 285, 1995, pp. 69–94.

[24]Lin, S. J., and Corcos, G. M., "The Mixing Layer: Deterministic Models of a Turbulent Flow. Part 3. The Effect of Plane Strain on the Dynamics of Streamwise Vortices," *Journal of Fluid Mechanics*, Vol. 141, 1984, pp. 139–178.

[25]Neu, J. C., "The Dynamics of Stretched Vortices," *Journal of Fluid Mechanics*, Vol. 143, 1984, pp. 253–276.

[26]Tobak, M., and Peake, D. J., "Topology of Three-Dimensional Separated Flows," *Annual Review Fluid Mechanics*, Vol. 14, 1982, pp. 61–85.

[27]Hunt, J. C. R., Abell, C. J., Peterka, J. A., and Woo, H., "Kinematical Studies of the Flows Around Free or Surface-Mounted Obstacles; Applying Topology To Flow Visualization," *Journal of Fluid Mechanics*, Vol. 86, 1978, pp. 179–200.

[28]Meyer, R., Bechert, D. W., Hage, M., and Montag, P., "BMBF-Vorhaben 13N6537-8 Aeroflexible Oberflächenklappen als 'Rückstrombremsen' nach dem Vorbild der Deckfedern des Vogelflügels," Abschluβbericht DLR IB 92517-97/B5, 1997.